



Advanced hybrid-structured anodes for lithium-ion batteries

Alexander Y. Galashev^{a,b,*}, Kseniya A. Ivanichkina^{a,b}, Oksana R. Rakhmanova^{a,b}

^a Institute of High-Temperature Electrochemistry, Ural Branch, Russian Academy of Sciences, Akademicheskaya Str. 20, Yekaterinburg 620990, Russia

^b Ural Federal University named after the first President of Russia B.N. Yeltsin, Mira Str., 19, Yekaterinburg 620002, Russia

ARTICLE INFO

Keywords:

Molecular dynamics
Nickel
Phosphorous doping
Silicene
Structure

ABSTRACT

Silicene is an artificially created two-dimensional silicon crystal with a hexagonal structure. Silicene layered product on a metal substrate is considered as the promising anode material for a lithium ion battery (LIB). The creation of polyvacancies in silicene can significantly reduce the charging time of the anode, and hence the entire battery, as well as increase the charging capacity of the device. However, the presence of polyvacancies reduces the mechanical strength of silicene. To strengthen defective silicene and increase its intercalation ability, it is proposed to carry out neutron transmutation doping of this two-dimensional material together with the substrate. In this work, the molecular dynamics method is used to study the strength of the doped and undoped two-layer silicene on a Ni(111) substrate when the interlayer space is filled with lithium. The morphology of silicene intercalated with lithium and the detailed structure of the lithium packing are investigated. The stresses appearing in the walls of the silicene channel when it is filled with lithium are calculated. A direct comparison of the properties characterizing the suitability of the two-layer silicene as a LIB anode is carried out for the corresponding doped and undoped systems.

1. Introduction

Silicon and tin are often used in the construction of the high-capacity anodes for metal-ion batteries. So, the composite SnS₂/C anodes tested in the K- and Na-ion batteries provides good intercalation characteristics [1,2]. A unique yolk-shell structure of Si/C composites has proven itself to be the high-performance anode material [3]. The outer carbon shell of this porous material does not impede a rapid passage of electrons and lithium ions, and also reduces the resistance to charge transfer and electrolyte corrosion.

This work considers the use of nanostructures capable of producing a high degree of lithium intercalation and having a large surface area. The high-capacity storage properties are created due to the formation of thin layers of lithium atoms at the surface of two-dimensional silicon. It is a well-known fact that all modern digital electronics are based on silicon. Silicon is also an essential material for photovoltaics and photonics. The pursuit of miniaturization in electronics requires new silicon materials, such as one-dimensional nanowires or nearly zero-dimensional nanocrystals. Great opportunities are also assigned to two-dimensional silicon.

Silicene is the monolayered silicon composed of hexagonal atomic

structures. Unlike graphene, silicene is not completely flat; conventionally, we can assume that Si atoms in silicene are at two different levels, and the silicene surface looks like ordered ripples. The big advantage of silicene over other two-dimensional materials is its compatibility with silicon semiconductor technologies. DFT calculations indicate a great similarity in some electronic properties of silicene and graphene [4]. At present, the silicene layer withdrawn from a vacuum is protected from the effects of the environment by a Al₂O₃ thin film [5]. Silicene is practically inseparable from the substrate, on which it was prepared. Therefore, the choice of a support substrate is critical for determining the scope of silicene application. In other words, silicene is integrated into the structure of the device together with the support substrate.

Graphite has a smaller surface area than silicon and has a low Li storage capacity. Silicon seems to be a significantly better anode material than graphite, since it has a higher capacity and more acceptable LIB cycling characteristics [6]. Currently used lithium-ion batteries do not meet the requirements of powering electric vehicles or integrated renewable energy sources. When creating new generation batteries, fundamental difficulties mainly associated with the choice of the LIB anode material were encountered. But this problem is not related to the

* Corresponding author at: Institute of High-Temperature Electrochemistry, Ural Branch, Russian Academy of Sciences, Akademicheskaya Str. 20, Yekaterinburg 620990, Russia.

E-mail address: galashev@ihte.uran.ru (A.Y. Galashev).

<https://doi.org/10.1016/j.commsci.2021.110771>

Received 23 March 2021; Received in revised form 7 July 2021; Accepted 1 August 2021

Available online 10 August 2021

0927-0256/© 2021 Elsevier B.V. All rights reserved.

resistance of the electrode or damage caused by exposure to the LIB electrolyte. Active materials with high capacities such as silicon have a large change in volume during cycling, which can reach up to 300% [7]. And although the theoretical capacity of silicon (~4200 mAh/g) is many times higher than the capacity of the traditionally used graphite anode material (372 mAh/g), crystalline silicon is not suitable for LIB [8]. A small number of charge/discharge cycles leads to crushing of the silicon anode and the LIB failure [9]. Besides, there is a problem associated with the formation of a solid electrolyte interfacial (SEI) layer as a result of the interaction between the electrolyte and the active material of the anode. An *ab initio* study of the interaction between lithium and single-layer silicene showed that the breaking of Si–Si bonds is the reason for the limitation (to 1196 mAh/g) of the capacity of silicene [10]. However, direct filling of the free-standing two-layer silicene with lithium showed that its charging capacity can reach 1384 mAh/g [11]. A schematic diagram of LIB with a silicene anode is shown in Fig. 1.

In order to maintain the stable power and voltage during operation of power devices, the silicon used in these devices has to be doped with impurities that create a higher current with less resistance and use more silicon volume. Physical doping of silicon materials with phosphorus is rather difficult to carry out due to the high energy for the impurity formation [12]. Thus, after the implantation of P^+ ions into a Si(100) target heated to temperatures of 600–1100 °C and after reaching the highest doping level, an intense diffusion of phosphorus to the surface and its subsequent evaporation into vacuum was observed [13]. In this case, in the range of $900 \leq T \leq 1100$ °C, the diffusion coefficient of phosphorus has an inverse temperature dependence. The ion implantation always imposes the risks of lattice defects or diffusion of undesirable impurity atoms into the material. For large silicon single crystals, it is usually difficult to obtain a material with a uniform impurity distribution. Using the method of neutron transmutation doping (NTD), it is possible to produce *n*-type single silicon crystals with a very uniform distribution of phosphorus in the bulk [14]. Also, the alloying element is created using the NTD method on the same lattice site of the original semiconductor material. This contributes to the significantly less defect formation than using other methods.

The electrical properties of semiconductors can be improved by performing the NTD procedure. In particular, in the case of silicon, this procedure is illustrated by the following reaction



where *n* is a neutron, *h* is an hour, and β^- is the beta radiation.

After absorbing a thermal neutron by the nucleus of the Si atom, it

transfers to the unstable state, which can lead to a change in the atomic number of an element due to the nuclear transmutation. As a result of a nuclear reaction with a short half-life of Si^{31} (about 2.62 h), phosphorus P^{31} is formed. Similarly, the thermal neutron irradiation of nickel can result in the formation of copper atoms in the metal.

This work aims to study the suitability of silicene on the nickel substrate doped by the NTD method as an anode material for LIB and to compare the performance of this material with the properties of the corresponding undoped and polyvacancy-filled silicene on a perfect nickel substrate.

2. Material and methods

To study the motion of the lithium ion along the silicene channels and the filling of such channels with lithium, a method of molecular dynamics (MD) simulation was used. The following systems were used. The flat channel was formed from two sheets of silicene, each of which, in the absence of defects, had a size of 4.1×4.8 nm and consisted of 300Si atoms. Silicene had a two-tier honeycomb flower structure. Its unit cell was formed by 18Si atoms, six of which were raised above the main plane by 0.074 nm. Such silicene structure is arranged on an Ag (111) substrate during the epitaxial growth [15]. Mono- and polyvacancies were approximately evenly distributed over the surface of the silicene sheets and were created by removing a certain number of atoms. Each sheet contained 9 vacancy defects and consisted of 291, 282, 273, and 252Si atoms after the formation of mono-, bi-, tri-, and hexavacancies in it, respectively. According to the DFT calculation [16], the formation energies for that vacancies are 2.610 eV, 3.217 eV, 4.768 eV, 8.860 eV, respectively.

The silicene sheets were aligned parallel to the horizontal *xy* plane with a slight offset in the *x* and *y* directions to form the *ABAB...* Bernal stacking. When silicene in the presence of monovacancies served as the channel walls, the motion of a single Li^+ ion through the channel was studied at the possible channel gap from 0.6 to 0.8 nm. However, when the channel walls contained various types of vacancy defects, the channel gap was 0.75 nm. The filling of the channel with lithium was studied at the constant optimal gap equal to 0.75 nm [17]. The substrate was formed from six (111) equally spaced nickel planes. One defect-free plane (111) consisted of 403 Ni atoms. The interatomic distances in the substrate were chosen the same as in the bulk nickel crystal. In particular, the interplanar distance was determined as 0.22 nm. The close-packed nickel layers had the *ABAB...* stacking. The initial distance between the lower silicene sheet and the upper substrate layer was 0.27 nm. An electric field having strengths of 10^4 and 10^5 V/m was used to

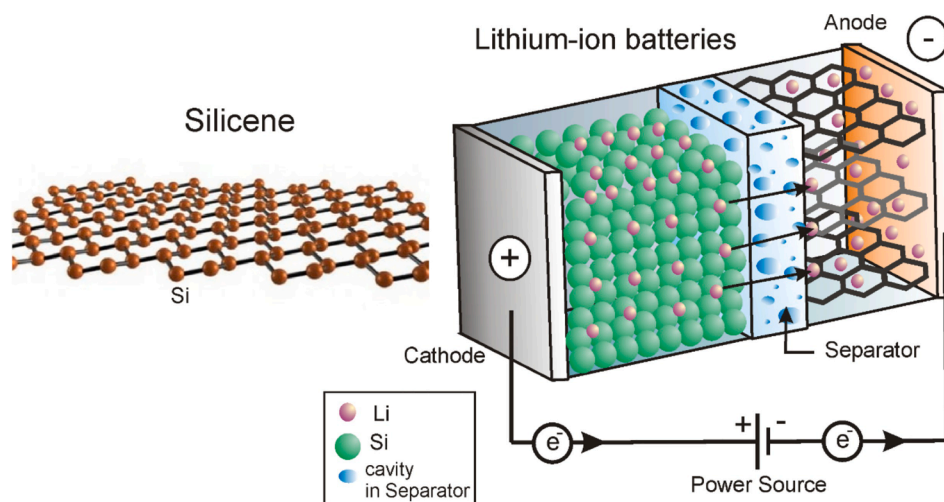


Fig. 1. Schematic diagram of charging LIB with a silicene anode, silicene is shown on the left, and a charged LIB is shown on the right; Li^+ ions rush to the anode; the legend shows individual LIB image elements; the cavities presented in the separator are necessary for the transfer of lithium ions.

study the motion of a single Li^+ ion along the silicene channel and with a strength of 10^4 V/m when the channel was filled with lithium.

Doping of silicene with phosphorus was carried out by filling mono- and polyvacancies with P atoms, i.e. by replacing the removed Si atoms with P atoms. Thus, we obtained 3%, 6%, 9%, and 18% phosphorus doping of silicene. Nickel was doped with copper by randomly selecting 5% of Ni atoms, which were replaced by Cu atoms. Further, based on the DFT calculations, it was shown that the stability of a doped silicene sheet on the modified nickel substrate increased as the phosphorus concentration raised [18]. So, the adhesion energy between the silicene sheet and the nickel substrate increased by $\sim 6.5\%$, and the total bond energy in the silicene sheet increases by $\sim 2.3\%$ when the phosphorous concentration in silicene grew from 0 up to 18%.

The interaction between Si atoms within each silicene sheet is described by the Tersoff potential [19], which adequately reproduces the thermodynamic, mechanical, and structural properties of this two-dimensional material [15,17,20,21]. The interaction between Si atoms belonging to different sheets of silicene has the character of a van der Waals interaction and is described by the Morse potential [20–24]. A modified EAM/Alloy potential [25] was used to describe the interactions Ni–Ni, Ni–Cu, and Cu–Cu in a metal substrate. All other interaction potentials were determined in quantum mechanical calculations in the form of the Morse potential [26,27].

All calculations were performed in an NVT ensemble using a Nose thermostat [28] at a temperature of 300 K. To solve the equations of motion, we used the “jumping frog” algorithm with a time step of $\Delta t = 1 \cdot 10^{-16}$ s. In this case, it is possible to avoid the appearance of “hot” particles in the systems, where various atoms with different types of interactions are present. Such particles can appear when the interparticle distances are incorrectly determined at a large time step.

It was experimentally shown that Li^+ ions behave differently in silicene than in graphite [29]. During the intercalation, the Li^+ ion (which is surrounded by Si atoms) acquires an electron quickly and becomes a neutral atom. The deintercalation process is associated with the capture of electrons by Li atoms from silicon. Then these atoms rush to the cathode in the form of ions.

The passing of the single lithium ion through the silicene channel was investigated when a single ion entered the channel from its front side (designated as F). Then, being pushed by an external electrostatic force, it performed the motion like Brownian one in the channel. Afterwards the ion left the channel passing through its back side (designated as B). The possible residence time of a single Li^+ ion in the silicene channel was limited to 100 ps. This time is 10 times longer than the ion lifetime in the next computer experiment (described in the present manuscript), where the filling of the channel with lithium was investigated. The filling of the silicene channel with lithium was carried out by introducing lithium ions into it periodically. The ions were introduced one after another in equal time intervals (10 ps) through the F side. The ion lifetime in the channel was 10 ps. After this time, the ion became an atom, i.e. it lost an electrical charge. In this case, the nature of its interaction with other atoms did not change, but the electric field stopped acting on it. Note, that the time of spontaneous emission of an electron according to the classical concept of the terahertz radiation is exactly 1 ps [30]. Thus, during the selected time interval (10 ps), the ion has a high probability of acquiring the missing electron and becoming an atom and vice versa.

Before performing the MD simulation of the single lithium ion passing and the silicene channel filling with lithium, the systems were equilibrated during 50 ps. Free boundary conditions were used in all calculations. On the one hand, this made it possible to determine accurately the filling of the silicene channel with lithium, since the exit of Li atoms from the channel was easily established. On the other hand, there was no need to introduce a background charge in order to avoid a discrepancy in the electrostatic potential and the interaction between the images.

Since silicene does not have a flat structure, bends on its surface may

be associated with roughness. The silicene channel was designed in such a way that the protrusions that form the flower structure were facing outward. The roughness of silicene was determined in the usual way as the arithmetic mean deviation of its surface profile [31]

$$R_a = \frac{1}{N} \sum_{i=1}^N |z_i - \bar{Z}|, \quad (2)$$

where N is the number of atoms, creating the silicene surface, z_i is the vertical displacement of the i atom (in the direction of the oz axis), \bar{Z} is the average coordinate of the entire silicene surface, z_i and \bar{Z} are determined simultaneously.

Methods for constructing Voronoi polyhedra (VP) [32] and combined polyhedra [33] were used to study the detailed structure of the lithium atoms packing in the silicene channels and to study the relief of the channel walls. In the latter case, Si atoms served as geometric neighbors, and the center of the polyhedron was represented by the Li^+ ion.

The virial stress tensor, which shows the degree of mechanical action on the material, can be represented in the following form [34]

$$\sigma_{\alpha\alpha}^V = \frac{1}{V} \sum_i \left[\frac{1}{2} \sum_j^N (r_u^j - r_\alpha^j) r_\alpha^{ij} - n_d k_B T \right] \quad (3)$$

where the indices u, α indicate the x, y, z directions; N is the number of neighbors affecting the i atom; the location of the i atom detected in the u direction is denoted as r_u^i , the force acting from the j atom on the i atom along the direction α is represented as f_α^{ij} ; the total volume of the system is given by the variable V ; the system has n_d degrees of freedom; k_B denotes the Boltzmann constant, and T denotes the absolute temperature.

To calculate the stress distribution, the silicene sheets were divided into elementary areas. We calculated the $\sigma_{\alpha\alpha}(l)$ stresses arising at each l elementary area with the orientation u as a result of the action of a force with the direction $\alpha (=x, y, z)$. All forces acting between atoms j and atom i and passing through the elementary area l are considered.

The bulk and shear moduli of perfect silicene calculated by us with the parameters of the Tersoff potential identical with this work have values of 136 and 59 GPa, respectively [27]. The DFT calculations for these values lead to the values of 112 and 69 GPa, respectively [35]. In this case, there is no tendency for the perfect single- and two-layer silicene to fracture with the lattice parameters (0.3855 and 0.384 nm) identical to [36]. The adhesion energy of free-standing silicene calculated by us (-4.48 eV/atom) is close to the corresponding value determined in the *ab initio* DFT simulation (-4.57 eV/atom) [37].

3. Results

3.1. Motion of a lithium ion in the channel of the modified system “two-layer silicene/nickel substrate”

The trajectories of the Li^+ ion along the silicene channels doped with phosphorus or containing monovacancy defects are shown in Fig. 2. In this case, the doping level of the silicene sheets is equal to 3%, and the monovacancies are the only defects. The gap between the silicene sheets varies from 0.6 nm (Fig. 2a and 2b) up to 0.75 nm (Fig. 2c and 2d). The initial positions for the Li^+ ion in all simulations were the same. The channels were located on the Ni(111) substrate. Moreover, in the case of doping of silicene with phosphorus, the nickel substrate was doped with copper. The substrate was not doped when the silicene had vacancy defects.

Fig. 2 shows that the walls of the silicene channel doped with phosphorus undergo less deformation than the channel walls containing monovacancies. This is due to the weakening of bonds within the sheet, which is associated with the presence of monovacancies in it. Since the bottom silicene sheet has a rigid support from the substrate and a

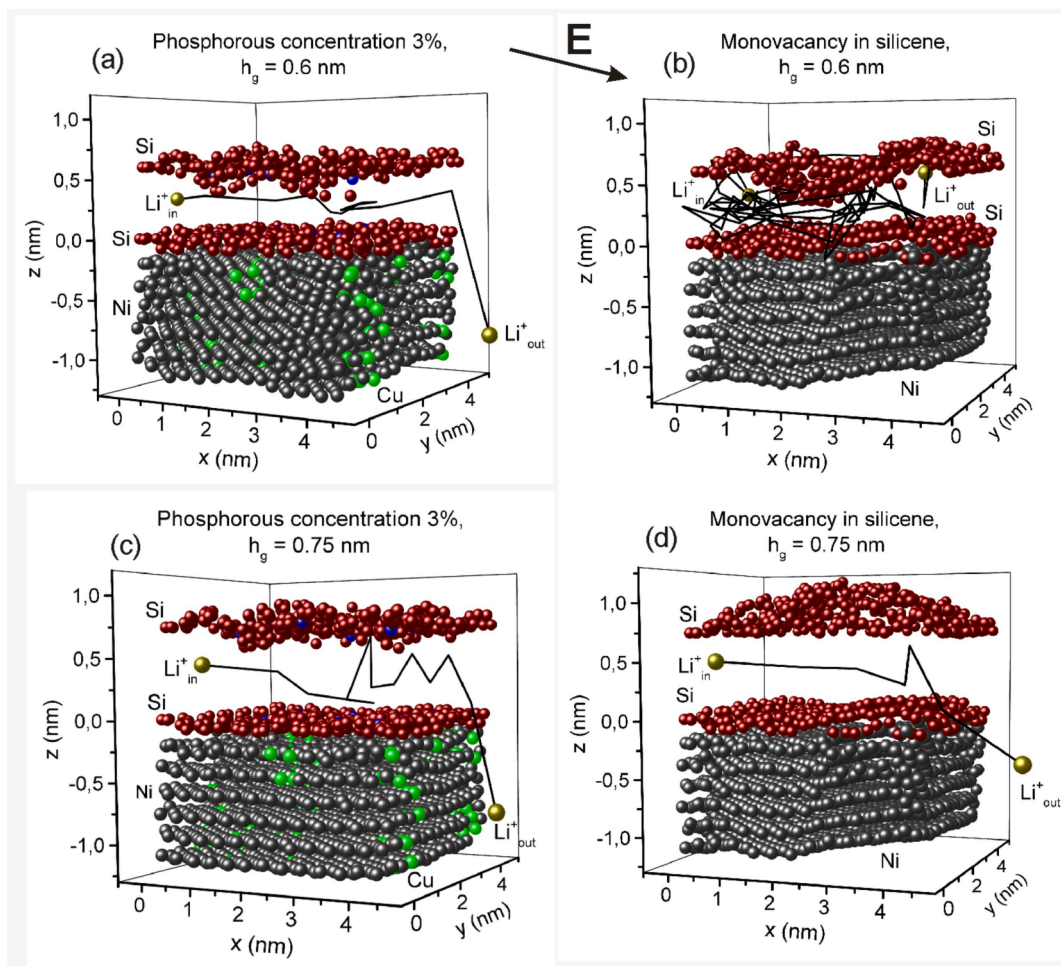


Fig. 2. Configurations of the “silicene channel on the Ni(111) substrate” system, which walls are 3% doped with phosphorus ((a) and (c)) or modified with monovacancy defects ((b) and (d)); broken lines show the trajectory of the lithium ion along the channel; the configurations correspond to the instant of 100 ps; the arrow shows the direction of the applied external field, $E = 10^4$ V/m.

sufficient value of the adhesion energy (~ 0.9 eV/atom) to it [17], the silicene layer adjacent to the substrate is always less bent than the top layer. In other words, since the surface of the Ni metal substrate is predominantly flat, even the existing Si–Ni bonds are sufficient to make the surface of the bottom silicene sheet almost flat. The top silicene layer is located rather far from the substrate (0.8–1.1 nm). Therefore, the weakened van der Waals bonds between the substrate and the top sheet do not have any significant effect on its geometry. As a result of interaction with the Li^+ ion, top layer acquires significantly greater distortions than the bottom one.

The permeability of the silicene channel by the Li^+ ion depends both on the channel gap width h_g and on the composition and structure of the channel walls. In the cases when the channel gaps are small ($h_g \leq 0.7$ nm) and when silicene is functionalized with monovacancies, a lithium ion can get stuck in the channel. Silicene binds well to the metal substrate. Not only does the substrate affect the silicene, but the silicene also affects the state of the substrate. It can be seen that in the presence of monovacancies, the lower silicene sheet experiences some bending when Li^+ ion moves along the channel. Due to the rather strong adhesion of silicene to the substrate, the shape of the bottom sheet of this material is transferred to the substrate, all layers of which are slightly curved (Fig. 3b and 3d). A slight curvature of the Ni(111) planes of the substrate, observed upon doping with copper, grows with an increase in the doping level from 6% to 9% (Fig. 3a and 3c).

The gap between the silicene sheets shown in Fig. 3 is equal to 0.75 nm. Phosphorous concentration varies from 6% up to 9%. The size of

defects in the silicene sheets increases from bivacancy up to trivacancy. One may see here the stabilizing function of phosphorus for silicene sheets (Fig. 3a and 3c) even when the P concentration is rather high (up to 9%). When the silicene sheets are functionalized with bi- and trivacancies (Fig. 3b and 3d), the shape of the top sheets bends significantly. The trajectory of Li^+ ion may be both “reactive” (Fig. 3a and 3d) and “slow” (Fig. 3b and 3c).

In the case of 6% phosphorus doping, the P atoms are located close to Si ones in silicene and do not create a strong roughness of the latter. This facilitates the rapid movement of the Li^+ ion along the channel. Deceleration of the Li^+ ion in a system heavily doped (up to 9%) with phosphorus is due to the vertical displacements of P atoms, which retard the movement of the ion towards the exit from the channel. If bivacancies are present in the channel walls, the Li^+ ion has strong deceleration due to a rather big distortion of the relief of the reflecting surfaces (channel walls) at the small channel gap. When silicene has trivacancy defects, a smoother change in the relief of the reflecting surfaces is observed, and the movement of the ion along the channel becomes more rapid.

Tables 1 and 2 show the time length of the lithium ion passage through the silicene channels, having the gaps from 0.6 nm to 0.8 nm with different types of vacancy defects (Table 1) and different concentrations of P doping (Table 2) of the silicene channel walls. As one may see from Tables 1 and 2, in all other cases, i.e. in the cases not described above, the silicene channel turns out to be passable for the ion. The calculations were carried out using two values of the electric field $E = 10^4$ and 10^5 V/m. The ion travels along a complex path in the silicene

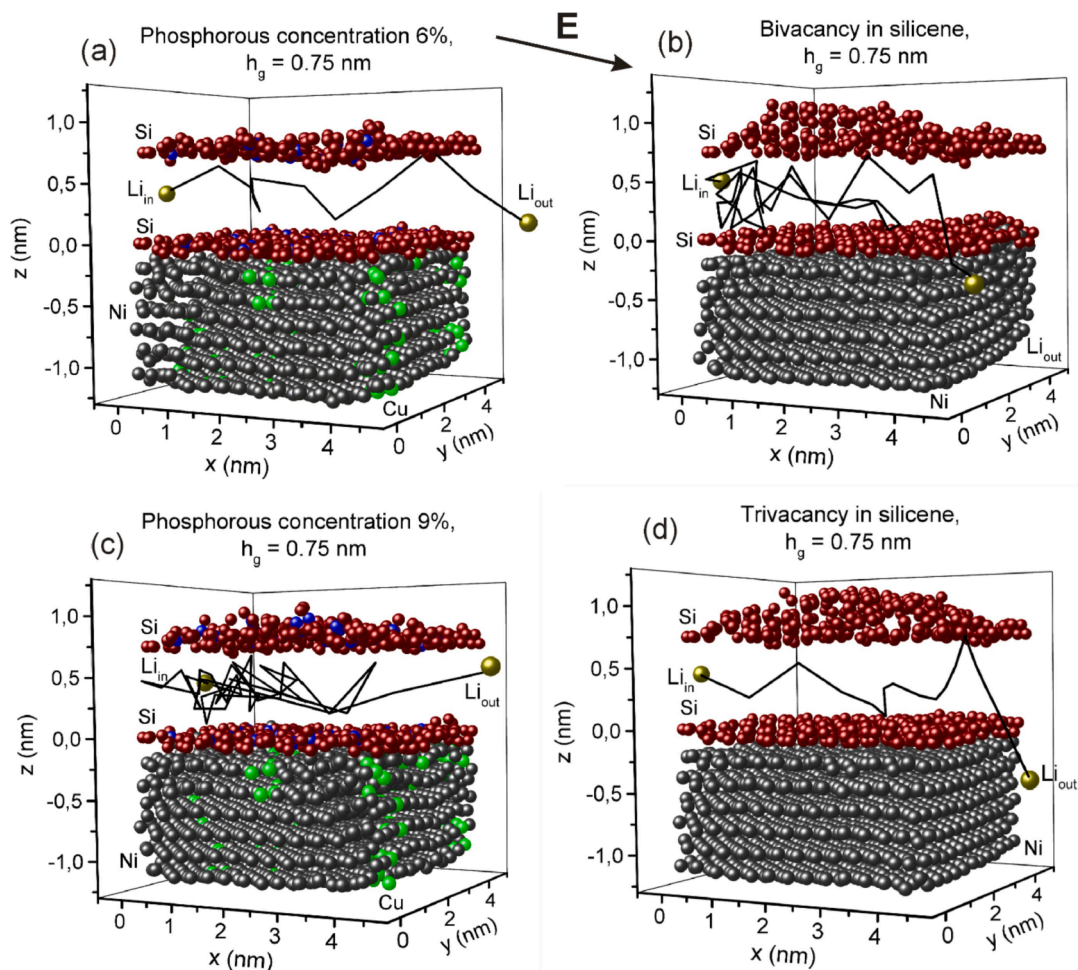


Fig. 3. Configurations of the “silicene channel on the Ni(111) substrate” system, which walls are 6% (a) and 9% (c) doped with phosphorus or modified with bivacancy (b) and trivacancy (d) defects; broken lines show the trajectory of the lithium ion along the channel; configurations correspond to the instant of 100 ps; the arrow shows the direction of the applied external field, $E = 10^4$ V/m, $h_g = 0.75$ nm.

Table 1

The exit time (t , ps) of a lithium ion from the silicene channel located on the Ni (111) substrate when silicene is functionalized with vacancy defects.

Channel gap, nm	Vacancy type in the silicene sheets	t , ps (provided $E = 10^4$ V/m)
0.6	Mono-vacancies	ion does not leave the channel
0.7	Mono-vacancies	ion does not leave the channel
0.75	Mono-vacancies	8
0.75	Bivacancies	37
0.75	Tri-vacancies	18
0.75	Hexa-vacancies	12
0.8	Mono-vacancies	40

channel, which depends on the condition of the channel walls and the gap between the silicene sheets. Therefore, there is no direct correlation between the electric field strength and the residence time of the ion in the channel.

Fig. 4 shows the horizontal xy -projections of the bottom sheet of the silicene channel with 3% doping of its walls at different time intervals. Already by the time instant of 30 ps, the atoms of the dopant, i.e. phosphorus, are completely pushed out from their initial locations onto the surface of the silicene sheet. Moreover, the resulting monovacancies are transformed in such a way that no voids remain on the sheet. As can be seen from the figure, each P atom is attached immediately to three Si

Table 2

The time (t , ps) required for a lithium ion to leave the phosphorus-doped silicene channel located on the Ni(111) substrate.

Channel gap, nm	The degree of doping with phosphorus of the silicene sheets	t , ps (provided $E = 10^4$ V/m)	t , ps (provided $E = 10^5$ V/m)
0.6	3%	11	19
0.7	3%	28	11
0.75	3%	65	14
0.75	6%	16	10
0.75	9%	12	46
0.75	18%	15	34
0.8	3%	14	56

ones. An increase in the phosphorus concentration in the silicene sheets to 9% also leads to its displacement from the vacancies; however, the voids, in this case, are not tightened, but the P atom still tends to group with three Si atoms (Fig. 5).

Fig. 6 shows the calculated roughness values of the doped sheets forming the silicene channel in comparison with the undoped ones. The latter were modified by vacancies of various sizes. The silicene sheets are placed on the doped and undoped Ni(111) substrates, respectively. Considering each size of the channel gap and all analyzed degrees of doping with phosphorus, the roughness of sheets of the undoped silicene is higher than that of the doped silicene. Moreover, the lower channel sheet is less rough than the upper one due to the influence of the

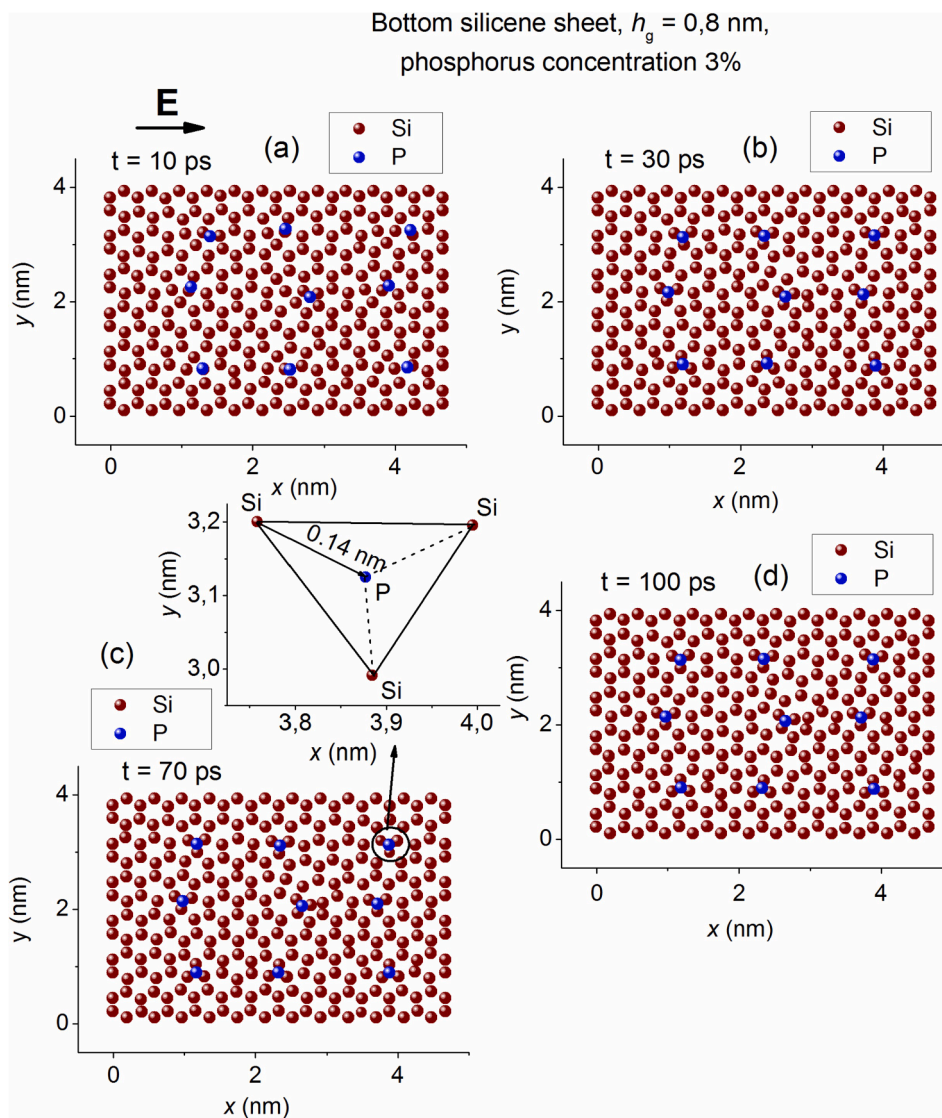


Fig. 4. Horizontal xy -projections of the bottom silicene sheet with 3% phosphorus doping at different time instants: (a) 10, (b) 30, (c) 70, and (d) 100 ps; an enlarged inset shows the relative position of Si and P atoms; the size of the gap of the silicene channel is 0.8 nm; the shown external electric field acts along the x axis.

substrate. As an example, the insets show zx -projections of the channel together with the upper substrate layer. When the channel walls are 3% phosphorus doped, its frontal profile is less curved than in the case when the channel walls contain monovacancies.

3.2. Simulation of lithization of the modified system “two-layer silicene/nickel substrate”

The number of lithium atoms filling the channel is always larger for the doped system than that for the undoped one (Table 3). Here, N_p is the percentage of phosphorus doping of silicene, N_{Li} is the number of lithium ions intercalated to the silicene channel. The maximum channel filling is achieved in the case of the 3% phosphorus doping or in the presence of monovacancies in the walls of the undoped silicene channel.

An example of the lithium-filled silicene channel with 3% P doping of the walls located on the Ni substrate with 5% Cu doping is shown in Fig. 7. The shape of the silicene channel and its filling with lithium is of interest. To depict them more clearly, the bottom three layers of the substrate, which do not influence the process, are not shown in the figure. It can be seen that the high filling of the channel is provided by the inward bending of the edges of its walls. The horizontal and vertical profiles of lithium density in channels with phosphorus-doped walls and

undoped walls containing polyvacancies are shown in Figs. 8 and 9, respectively. It is seen that doping with phosphorus makes it possible to obtain more uniform horizontal distributions of Li atoms in the channel. However, at a very high doping level, the uniformity of the arrangement of lithium atoms along the channel length disappears. In this case, three peaks are found in the horizontal density profile. The vertical density profiles show a high concentration of Li atoms in the central region of channels with doped walls. However, when the phosphorus doping level reaches 18%, the density profile broadens due to the occupation of the cavities in the channel walls by Li atoms.

3.3. Study of modified systems filled with lithium by the method of statistical geometry

Since silicene located on the nickel substrate does not have an ideal flat shape for a Li^+ ion moving along the channel, it is possible to construct three-dimensional Voronoi polyhedra (VP). The faces of such polyhedra are formed by adjacent Si atoms. Due to the small values of the z -coordinate (the z -axis is perpendicular to the plane of the substrate), such polyhedra will not have a high degree of symmetry. The packing of Li atoms in silicene can also be investigated by constructing the VP. In this case, VP were constructed only for Li atoms, i.e. the faces

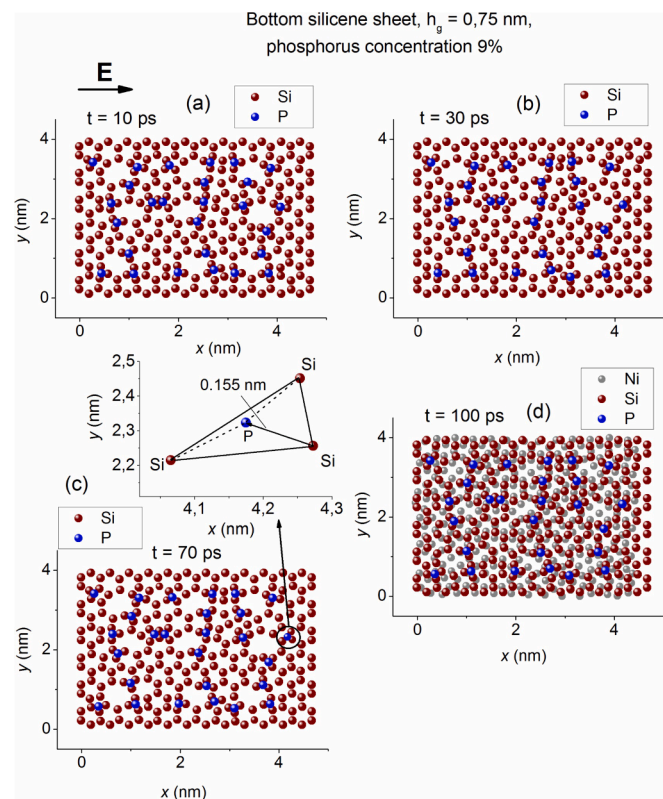


Fig. 5. Horizontal xy -projections of the bottom silicene sheet with 9% phosphorus doping at different time instants; (a) 10, (b) 30, (c) 70, and (d) 100 ps; an enlarged inset shows the relative position of Si and P atoms; the size of the gap of the silicene channel is 0.75 nm; the xy -projection of the sheet (bottom right) also shows the atoms of the upper layer of the Ni(111) substrate after 100 ps; the external electric field E acts along the x axis.

of the VP were formed by neighboring Li atoms.

The angular distribution (θ distribution) of the nearest geometric neighbors serves as an excellent tool for identifying the crystal structures in the MD model. In particular, by the intensity and location of the sharp peaks in this distribution, one can distinguish FCC, BCC and HCP structures [38–41]. Distortion of the structure associated with the presence of defects in the crystal leads to the appearance of a background in the θ spectrum.

The distribution of angles formed by Si neighbors with the Li^+ ion as it moves through channels with the gap of 0.75 nm is shown in Fig. 10. It is noteworthy that in all cases, most of the θ angles are concentrated in the vicinity of 90° . This θ value assumes that the ion spends most of the time near one of the channel walls, or it is sufficiently strongly bound to any of the channel walls. In contrast to the usual θ spectra obtained for three-dimensional atomic packings, the θ distributions obtained when the Li^+ ion moves along the channel are short and, as a rule, break off near the angle of $\theta = 90^\circ$. The θ distribution obtained as a result of the ion movement along the channel with walls heavily doped with phosphorus (18%) is an exception. In this case, the distribution is blurred and its “tail” expressed by bursts of extremely low intensity extends to the value of $\theta = 168^\circ$. This is due to the displacement of P atoms in the channel, i.e. the emerging three-dimensional structure in the system influences significantly the shape of the angular distribution.

The θ distributions for packings of Li atoms in the silicene channels with P-doped walls and with the walls containing polyvacancies for intercalation cases are shown in Fig. 11. As can be seen from this figure, the shapes of the θ spectra for the doped system and the undoped system differ insignificantly. The most dramatic difference is the stronger drop of the first peak of this distribution of the doped system. On average, the decrease in the intensity of this peak from the position of the maximum

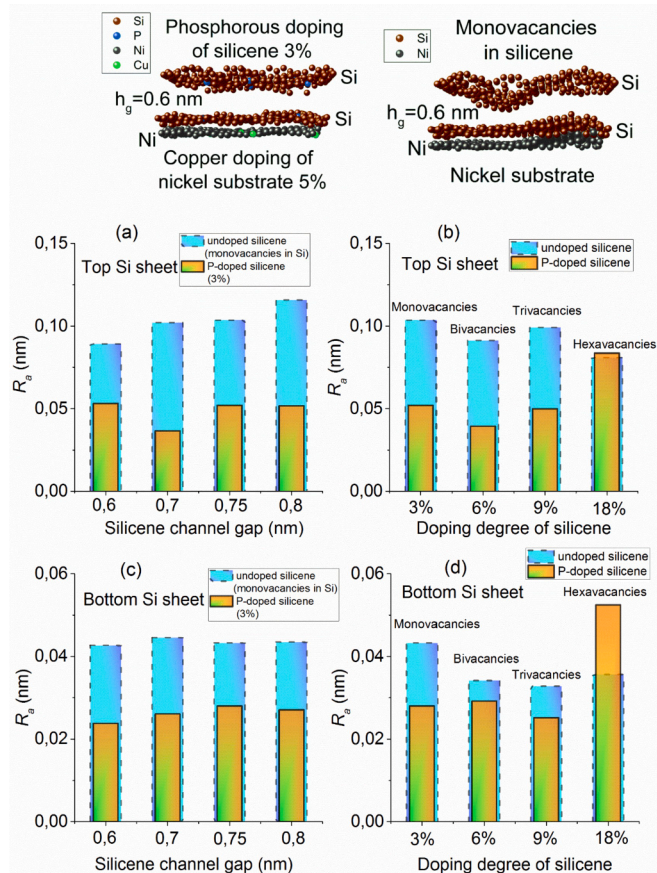


Fig. 6. The calculated values of the roughness of the silicene channel sheets depending on the size of the channel gap (a, c) and the degree of doping of its walls with phosphorus (orange bars) or on the size of vacancies (blue bars) (b, d); the upper insets show the zx -projections of the silicene channel (doped with phosphorus or modified with vacancies) and the top sheet of the Ni(111) substrate.

Table 3

The total number of Li atoms successfully incorporated into the silicene channel in the case of the doped and undoped systems*.

N_p	N_{Li} (doped system)	Defect type	N_{Li} (undoped system)
3%	140	monovacancies	122
6%	102	bivacancies	83
9%	119	trivacancies	81
18%	104	Hexavacancies	66

* N_p is the degree of phosphorus doping of silicene; N_{Li} is the number of lithium ions intercalated to the silicene channel.

up to the angle of 90° for the doped systems is 35% stronger than that for the systems containing polyvacancies in the walls of the silicene channel. The smaller dispersion of the first peak observed for doped systems indicates a more definite character of the arrangement of low-angle neighbors in lithium packings. Other topological and metric characteristics obtained by constructing VP for packings of Li atoms in channels are shown in Figs. S1–S3.

The distribution of normal stresses in the silicene sheets has a zig-zag shape when the channels are filled with lithium (Fig. 12). Moreover, the teeth of the zig-zag line have different heights, it is associated with the different degrees of local tension. From the viewpoint of the material strength, the fluctuation range, or the height of the teeth matters. In this respect, the silicene sheets doped with phosphorus are more reliable, because the range of fluctuations of the normal stress for them is much lower. Also, the maximum absolute stresses for them are much lower

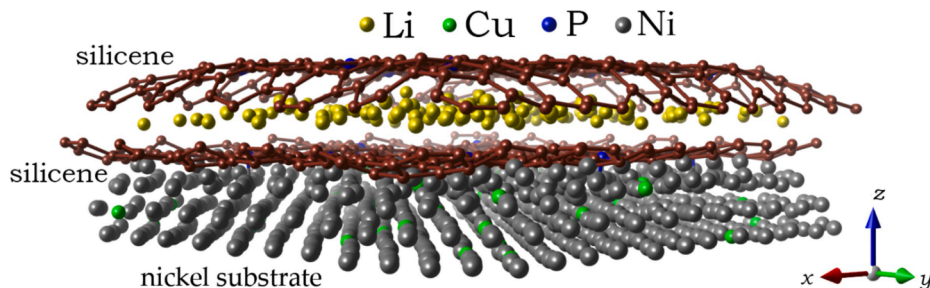


Fig. 7. A lithium-filled channel with a 0.75 nm gap between the silicene sheets after 150 ps from 3% phosphorus doping; a Ni substrate with 5% doping with Cu is used; the figure shows only the three closest to the silicene channel layers of the metal substrate.

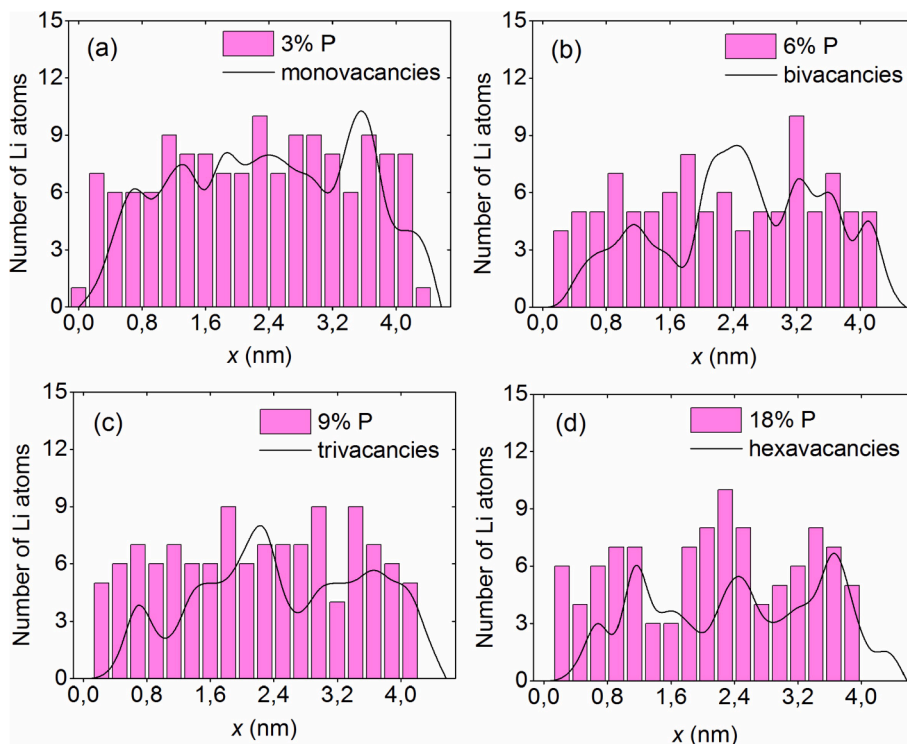


Fig. 8. Horizontal profiles of lithium density in the silicene channels at the final stage of intercalation; the histograms show the distributions corresponding to the systems with different degrees of doping, the lines show undoped systems with different content of vacancy defects: (a) – 3% P (monovacancies), (b) – 6% P (bivacancies), (c) – 9% P (trivacancies), (d) – 18% P (hexavacancies); the strength of the applied electric field is 10^4 V/m.

than those for the silicene sheets containing vacancy defects.

4. Discussion

All results obtained in this work are important for the forthcoming design of silicene anodes for LIB. They cannot be obtained by any other means than a computational experiment. The motion of a single Li^+ ion in the narrow flat silicene channel in the presence of a constant electric field is considered. Although the initial shape of the silicene sheets and the channel gap were directed to the rectilinear motion of the ion under the action of a constant electric force eE , such motion was not realized for any of the considered gaps and electric field strengths. The similarity of the ion motion along the channel with the Brownian one is explained by the influence of the interaction between the deformed channel walls and the ion. But there is a tendency for the ion to move towards the channel exit, i.e. in the direction opposite to the channel entrance. Even with a moderate phosphorus doping, the channel walls are straightened. As a result, the ion could pass a very narrow channel along a straighter trajectory than in the absence of doping. The degree of randomness of the interaction between the ion and the channel walls is enhanced at a

high doping level. Therefore, even with an increase in the gap of the channel with highly doped walls, the trajectory of the ion can become more entangled than that in the channel with the walls modified by polyvacancies.

At any of the considered doping levels, the P atoms do not remain in the positions of the Si atoms, which they replace. Depending on the initial vertical level of the location of the P atom, it shifts to the inner or outer surface of the channel wall. In this case, the P atom seeks to establish bonds with three Si atoms at once, which is explained by the following reasons. It has been shown experimentally that the strength of the Si–P bond is higher than the strength of the Si–Si one [42]. The binding energy decreases in the sequence Si–P, Si–Si, P–P as 3.1, 2.3, and 2.08 eV, respectively [27]. A single Si–P bond cannot be formed due to its high reactivity. Typically, suitable polar compounds break this bond. The Si = P double bonds are much more stable. Therefore, with a high probability, the pentavalent P atom turns out to be bonded to three Si atoms. The presence of the P atom over the center of the hexagonal Si-ring is unlikely since it is caused by the formation of single Si–P bonds.

The roughness of the silicene sheet decreases after doping with phosphorus if the doping level is not too high. At an extremely high 18%

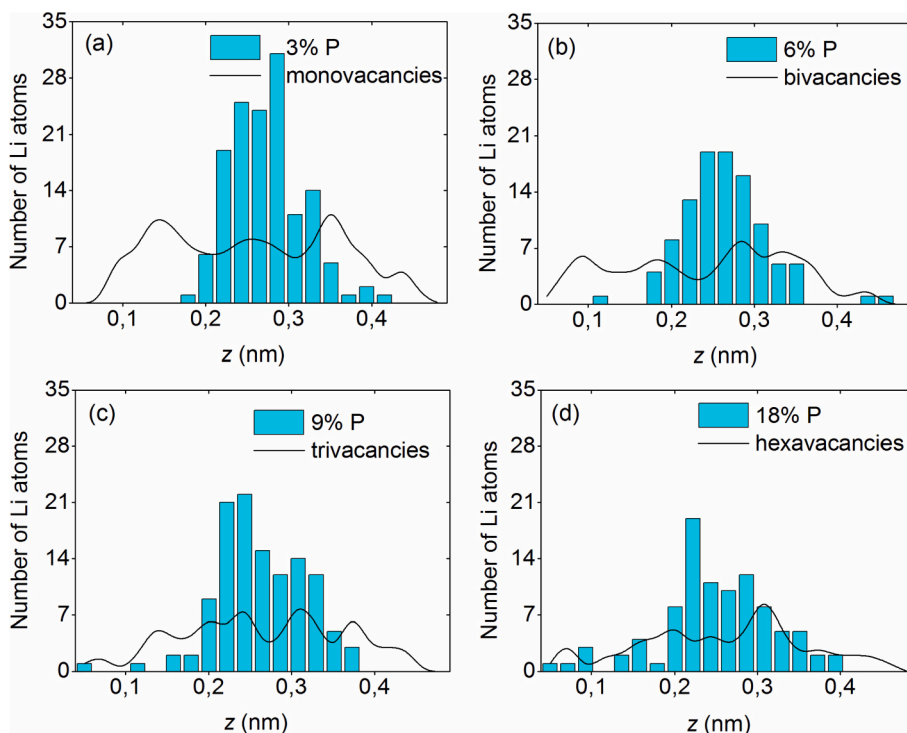


Fig. 9. Vertical profiles of lithium density in the silicene channels at the final stage of intercalation; the histograms show the distributions corresponding to the systems with different degrees of doping, the lines show undoped systems with different content of vacancy defects: (a) 3% P (monovacancies), (b) 6% P (bivacancies), (c) 9% P (trivacancies), (d) 18% P (hexavacancies); the strength of the applied electric field is 10^4 V/m.

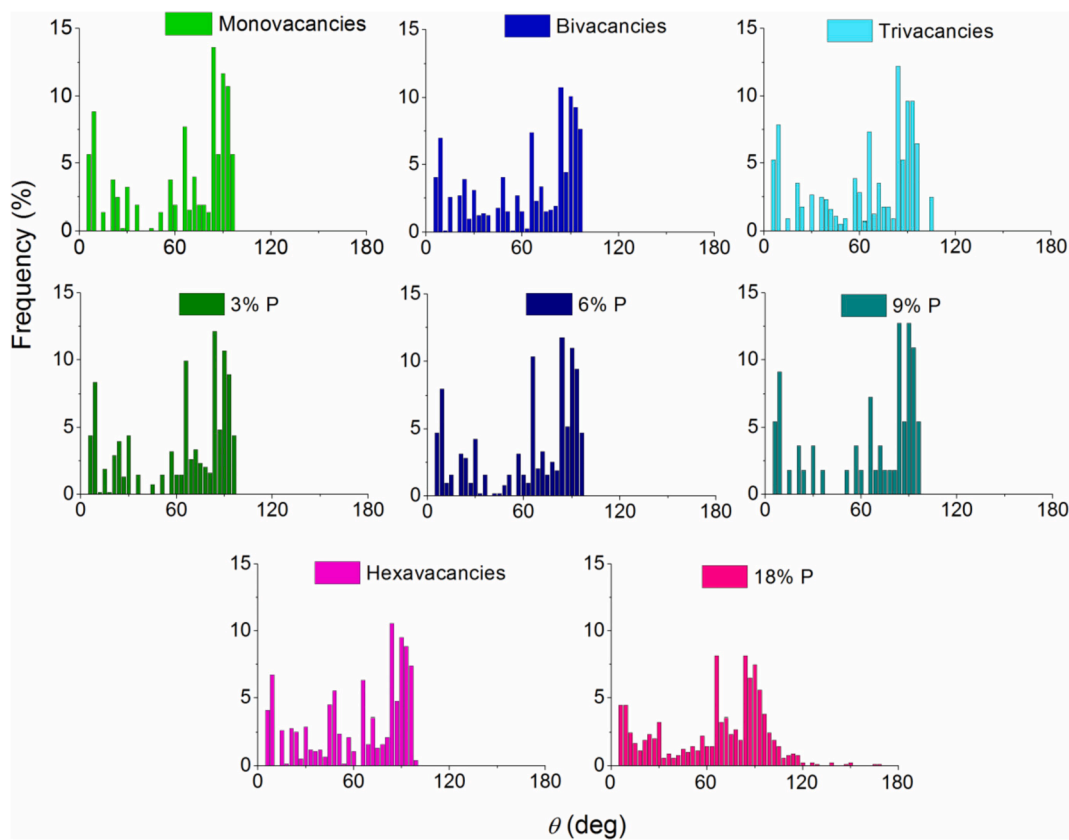


Fig. 10. Angular distributions of the nearest geometrical neighbors of a lithium ion during its movement along the silicene channels with polyvacancies and the channels with walls doped with phosphorus; the channels are located on the nickel substrate modified with Cu; the channel gap is 0.75 nm; the strength of the applied electric field is 10^4 V/m.

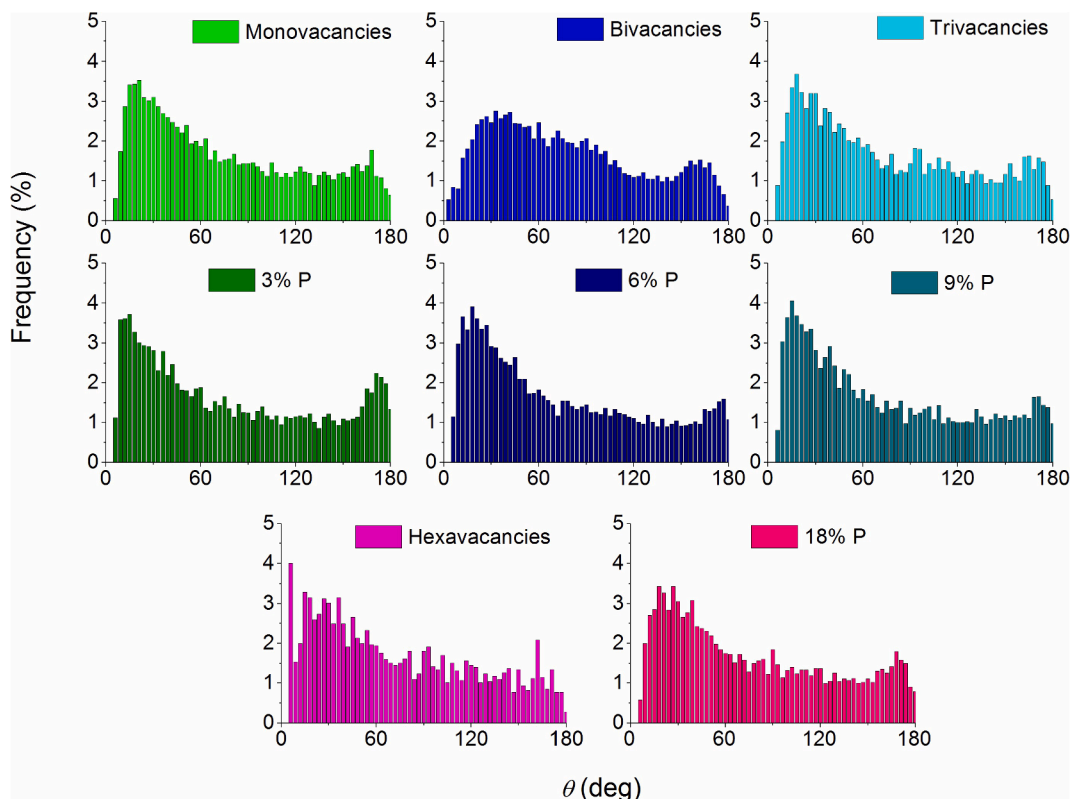


Fig. 11. Angular distributions of the nearest geometrical neighbors in lithium packings at the final stage of intercalation into the silicene channels with polyvacancies and into the channels with walls doped with phosphorus; the channels are located on the nickel substrate modified with Cu.

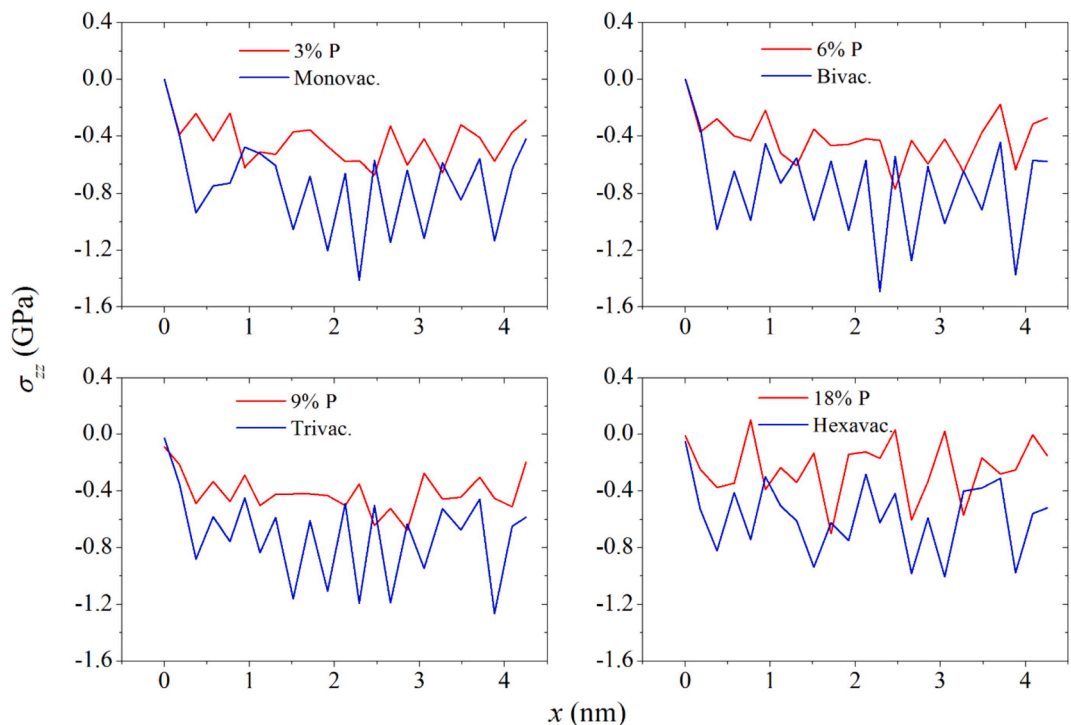


Fig. 12. Distribution of average normal stresses appearing in the silicene sheets when the channel is filled with lithium along the x (zig-zag) direction; the elementary platforms are elongated along the y -axis (armchair); the blue line presents the stresses in the channel walls with vacancy defects, the red line corresponds to the doped system.

doping, the proportion of P–P bonds, which are weaker than the Si–P ones, becomes rather big. This level of doping turns out to be ineffective. The doped silicene has a high tendency to fracture like silicene with an 18% of hexavacancies.

The channel formed by the phosphorus-doped silicene sheets is more densely filled with lithium than the channel with walls containing corresponding vacancy defects. Substituting Si atoms into P ones straightens and strengthens the silicene sheets. In this case, the volume of the channel increases and it becomes more accommodating for lithium atoms. The sheets are bent inside the channel only along their edges. The central surface of the sheets remains flat. The channel of this shape holds more lithium atoms.

The calculated horizontal packing densities of lithium in the channel indicate a fairly uniform filling of the channel with this metal in the direction of the applied electric field. The vertical density profiles show that the arrangement of lithium atoms is quite symmetric concerning the level of the channel gap half-width. Thus, the channel is sufficiently homogeneous and densely filled with lithium atoms during the intercalation. Such arrangement of Li atoms cannot be achieved when the silicene walls of the channel contain polyvacancies [43–46]. The presence of polyvacancies in the channel walls leads to its strong deformation when the channel is filled with lithium. That is why such channels are occupied less during the lithium intercalation.

Tracking the structure of the inner surface of the channel attracting the Li^+ ion was performed using the method of constructing combined polyhedra. The center of such polyhedron corresponds to the location of the moving ion. The geometric neighbors are found among the Si atoms forming the channel walls. The distribution of θ angles formed by pairs of neighbors with vertices located in the center of the polyhedron indicates that the ion spends most of the time near one of the channel walls. This behavior of the Li^+ ion is observed both in the channels with walls, modified by vacancy defects, and in the channels with the phosphorus-doped walls.

The packing structure of lithium atoms in the channels was investigated by constructing Voronoi polyhedra. The centers of the polyhedra and geometric neighbors were represented by Li atoms. The obtained angular distributions indicate a predominantly irregular packing of lithium atoms in the channels with walls of both types. The shape of these distributions differs from the shape of the corresponding distributions for one- and two-component liquids and crystals [38,40,47], as well as for various clusters [48,49]. This difference is due to the presence of two bounding surfaces, which were initially flat.

The stresses that appear on the silicene sheets are associated with a violation of the correct arrangement of atoms. The order in the arrangement of atoms is disturbed both by the presence of vacancy defects, due to the rearrangement of the structure associated with the displacement of atoms of the dopant (P), and also by the effect of lithium atoms filling the silicene channel. When the channels are filled with lithium, the strongest normal stresses arise in the silicene sheets containing vacancy defects. Elastic stresses grow in the silicene sheets at the transition from monovacancies to bivacancies. The calculations were performed without taking into account the decrease in the area of an elementary fragment, caused by the presence of a vacancy defect or its part. Actual local stresses can rise with an increase in the size of vacancy defects. However, the growth of defects leads to a decrease in the elasticity of the material. Therefore, the distribution of local stresses at a larger size of defects can be considered only as a qualitative characteristic. Nevertheless, even with 18% doping or the presence of hexavacancies in the silicene sheets, despite the equalization of the amplitude of σ_{zz} fluctuations in both cases the absolute values of this characteristic are higher when hexavacancies are present in the walls of the silicene channel. As can be seen from Fig. S4 and S5, the absolute magnitude of the σ_{zy} bursts can reach the value of the local stress σ_{zz} , but the σ_{zx} stresses always have lower values. Note that in all cases, the stresses present in the silicene sheets are significantly lower than the tensile strength of silicene (12.5 GPa) [50].

The value of molecular dynamics modeling of the lithium intercalation process is explained by the following circumstances. First, due to the usual excessive reduction of structural data obtained from X-ray crystallography, it is difficult to reproduce the three-dimensional picture of the packing of lithium atoms and to understand the peculiarities of packing of these atoms near the walls of the silicene channel. Second, the data of scanning electron microscopy, due to the specificity of the method, do not give a sufficiently accurate idea on the bending deformations observed in silicene during intercalation. Therefore, it is not an easy task to make an accurate morphological analysis of the silicene surface. Third, with the help of transmission electron microscopy, it is difficult to determine the true completeness of lithium filling the silicene channel. Finally, it is extremely difficult to reveal experimentally the stresses arising in the walls of the silicene channel when it is filled with lithium. The molecular dynamics modeling has a predictive value and allows, without carrying out complex and expensive physical experiments, establishing important structural and mechanical parameters of lithium intercalation to evaluate the functional characteristics of silicene.

Phosphorus is pentavalent, i.e. it has five electrons in its outer shell. When silicon (or silicene) is doped with this element, four electrons of the P atom bind to the Si atom. The fifth electron gains freedom to move and becomes a charge carrier. Phosphorus acts here as a donor. The n -type doping transforms silicon into a semimetal, where electrons are the main charge carriers. Lithium ions entering the phosphorus-doped silicon anode acquire the missing electron much more easily. This results in an increase in the LIB charging speed. Thus, in addition to strengthening the silicene and increasing the electrode capacity, phosphorus doping makes it possible to accelerate the LIB charging. The main disadvantage of silicene doping with phosphorus is the high diffusion coefficient of P atoms, which easily leave their initial locations and, hence, may rearrange the entire structure of silicene. The situation could be corrected by silicene doping with another heavier pentavalent element, for example, arsenic. However, this is much more difficult to accomplish due to the lack of the possibility of performing neutron transmutation doping with arsenic.

5. Conclusions

Nickel-supported silicene subjected to the NTD procedure was tested as an anode material for LIB using molecular dynamics simulation. The simulation of the Li^+ ion motion along the silicene channel modified with phosphorous and the channel with the silicene walls containing vacancy-type defects elucidated that at 6% phosphorus doping of the walls of the silicene channel provides the fastest passage of the channel by a single lithium ion. The calculations show that 3% phosphorus doping allows reaching the maximum filling level of the channel with lithium.

Phosphorus atoms leave quickly their initial locations (inside vacancy defects), penetrate the channel, or, conversely, are placed outside the channel. As a rule, each of them is grouped around three Si atoms. The horizontal density profiles indicate a significantly more uniform distribution of Li atoms in the channels with doped walls as compared to the channels with the undoped walls containing polyvacancies. The vertical density profiles broaden when the doping level of the channel walls increases. Doping of the channel walls with phosphorus provides a significantly greater occupation of the central region of the channel with lithium atoms.

The roughness of the lower silicene sheets directly in contact with the substrate is significantly lower than the roughness of the upper sheets. Before the onset of destruction of the channel walls, the roughness of the undoped silicene sheets containing hexavacancies turns out to be higher than the roughness of the 18% phosphorus-doped silicene sheets. A study of the detailed structure of the walls of the silicene channel showed that a single lithium ion most of the time moves near the channel walls; as a result, the angular distributions of its Si neighbors do not

extend to angles greater than 100°. The mechanical stresses appearing in the walls of the silicene channel during lithium intercalation are small and do not impose restrictions on the use of silicene as an electrode material.

Thus, the NTD procedure improves significantly the mechanical and electrochemical properties of the two-layer silicene on the nickel substrate and allows using this material as a LIB anode more effectively.

6. Data availability

All the scripts to reproduce the data in this article are freely available upon request from the corresponding author.

CRediT authorship contribution statement

Alexander Y. Galashev: Conceptualization, Methodology, Supervision, Investigation, Writing – original draft. **Kseniya A. Ivanichkina:** Data curation, Investigation, Software, Visualization, Writing – original draft. **Oksana R. Rakhmanova:** Data curation, Investigation, Software, Visualization, Writing – original draft.

Declaration of competing interest

The authors declare that they have no known competing financial interests or personal relationships that could have appeared to influence the work reported in this paper.

Appendix A. Supplementary data

Supplementary data to this article can be found online at <https://doi.org/10.1016/j.commatsci.2021.110771>.

References

- J. Liu, X.u. Yu, J. Bao, C.-F. Sun, Y. Li, Carbon supported tin sulfide anodes for potassium-ion batteries, *J. Phys. Chem. Solids* 153 (2021) 109992, <https://doi.org/10.1016/j.jpcs.2021.109992>.
- X. He, J. Liu, B. Kang, X. Li, L. Zeng, Y. Liu, J. Qiu, Q. Qian, M. Wei, Q. Chen, Preparation of SnS₂/enteromorpha prolifera derived carbon composite and its performance of sodium-ion batteries, *J. Phys. Chem. Solids* 152 (2021) 109976, <https://doi.org/10.1016/j.jpcs.2021.109976>.
- T. Shao, J. Liu, L. Gan, Z. Gong, M. Long, Yolk-shell Si@void@C composite with Chito-oligosaccharide as a C-N precursor for high capacity anode in lithium-ion batteries, *J. Phys. Chem. Solids* 152 (2021) 109965, <https://doi.org/10.1016/j.jpcs.2021.109965>.
- R. Qin, W. Zhu, Y. Zhang, X. Deng, Uniaxial strain-induced mechanical and electronic property modulation of silicene, *Nanoscale Res. Lett.* 9 (2014) 521–526, <https://doi.org/10.1186/1556-276X-9-521>.
- A. Molle, C. Grazianetti, D. Chiappe, E. Cinquanta, E. Cianci, G. Tallarida, M. Fanciulli, Hindering the oxidation of silicene with non-reactive encapsulation, *Adv. Funct. Mater.* 23 (35) (2013) 4340–4344, <https://doi.org/10.1002/adfm.2013030354>.
- S. Mozghan, S. Talebi, I. Kazeminezhad, J. Behestian, Theoretical prediction of silicene as a new candidate for the anode of lithium-ion batteries, *Phys. Chem. Chem. Phys.* 17 (2015) 29689–29696, <https://doi.org/10.1039/c5cp04666a>.
- J. Graetz, C.C. Ahn, R. Yazami, B. Fultz, Highly reversible lithium storage in nanostructured silicon, *Electrochem. Solid State Lett.* 6 (2013) A194–A197, <https://doi.org/10.1149/1.1596917>.
- A.Y. Galashev, K.A. Ivanichkina, K.P. Katin, M.M. Maslov, Computer test of modified silicene/graphite anode for lithium-ion batteries, *ACS Omega* 5 (2020) 13207–13218, <https://doi.org/10.1021/acso.0c01240>.
- U. Kasavajula, C. Wang, A.J. Appleby, Nano- and bulk-silicon-based insertion anodes for lithium-ion secondary cells, *J. Power Sources* 163 (2) (2007) 1003–1039, <https://doi.org/10.1016/j.jpowsour.2006.09.084>.
- S. Xu, X. Fan, J. Liu, D.J. Singh, Q. Jiang, W. Zheng, Adsorption of Li on single-layer silicene for anodes of Li-ion batteries, *Phys. Chem. Chem. Phys.* 20 (13) (2018) 8887–8896, <https://doi.org/10.1039/c7cp08036k>.
- A.Y. Galashev, K.A. Ivanichkina, Computer study of silicene applicability in electrochemical devices, *J. Struct. Chem.* 61 (2020) 659–667, <https://doi.org/10.1134/S0022476620040204>.
- G.M. Dalpian, J.R. Chelikowsky, Self-purification in semiconductor nanocrystals, *Phys. Rev. Lett.* 96 (2006) 226802–226806, <https://doi.org/10.1103/PhysRevLett.96.226802>.
- G.A. Kachurin, I.E. Tyschenko, A.P. Mazhirin, E. Wieser, High-temperature phosphorus ion doping of silicon, *Nuclear Instruments Methods Phys. Res. Section B: Beam Interactions Mater. Atoms* 43 (4) (1989) 535–538, [https://doi.org/10.1016/0168-583X\(89\)90403-5](https://doi.org/10.1016/0168-583X(89)90403-5).
- A.E. Galashev, A.S. Vorob'ev, Electronic properties of silicene films subjected to neutron transmutation doping, *Semiconduct.* 54 (2020) 641–649, <https://doi.org/10.1134/S1063782620060068>.
- S.K. Das, D. Roy, S. Sengupta, Volume change in some substitutional alloys using Morse potential function, *J. Phys. F: Metal. Phys.* 7 (1) (1977) 5–13, <https://doi.org/10.1088/0305-4608/7/1/011>.
- S. Li, Y. Wu, Y. Tu, Y. Wang, T. Jiang, W. Liu, Y. Zhao, Defects in silicene: vacancy clusters, extended line defects, and di-adatoms, *Sci. Rep.* 5 (2015) 7881, <https://doi.org/10.1038/srep07881>.
- A.Y. Galashev, K.A. Ivanichkina, Silicene anodes for lithium-ion batteries on metal substrates, *J. Electrochem. Soc.* 167 (5) (2020) 050510, <https://doi.org/10.1149/1945-7111/ab717a>.
- A.Y. Galashev, K.A. Ivanichkina, A.S. Vorob'ev, O.R. Rakhmanova, K.P. Katin, M.M. Maslov, Improved lithium-ion batteries and their communication with hydrogen energy, *Int. J. Hydr. Ener.* 46 (2021) 17019–17036, <https://doi.org/10.1016/j.ijhydene.2020.11.225>.
- J. Tersoff, Modeling solid-state chemistry: Interatomic potentials for multicomponent systems, *Phys. Rev. B: Condens. Matter.* 39 (8) (1989) 5566–5568, <https://doi.org/10.1103/PhysRevB.39.5566>.
- A.E. Galashev, O.R. Rakhmanova, Y.P. Zaikov, Defect silicene and graphene as applied to the anode of lithium-ion batteries: numerical experiment, *Phys. Solid State* 58 (9) (2016) 1850–1857, <https://doi.org/10.1134/S1063783416090146>.
- A.E. Galashev, K.A. Ivanichkina, A.S. Vorob'ev, O.R. Rakhmanova, Structure and stability of defective silicene on Ag(001) and Ag(111) substrates: A computer experiment, *Phys. Solid State* 59 (6) (2017) 1242–1252, <https://doi.org/10.1134/S1063783417060087>.
- A.Y. Galashev, K.A. Ivanichkina, Nanoscale simulation of the lithium ion interaction with defective silicene, *Phys. Lett. A* 381 (36) (2017) 3079–3083, <https://doi.org/10.1016/j.physleta.2017.07.040>.
- A.E. Galashev, K.A. Ivanichkina, O.R. Rakhmanova, Y.P. Zaikov, Physical aspects of the lithium ion interaction with the imperfect silicene located on a silver substrate, *Lett. Mater.* 8 (4) (2018) 463–467.
- A.E. Galashev, K.A. Ivanichkina, Numerical simulation of the structure and mechanical properties of silicene layers on graphite during the lithium ion motion, *Phys. Solid State* 61 (2) (2019) 233–243, <https://doi.org/10.1134/S1063783419020136>.
- S.M. Foiles, M.I. Baskes, M.S. Daw, Embedded-atom-method functions for the fcc metals Cu, Ag, Au, Ni, Pd, Pt, and their alloys, *Phys. Rev. B: Condens. Matter, Mater. Phys.* 33 (12) (1986) 7983–7991, <https://doi.org/10.1103/PhysRevB.33.7983>.
- A.Y. Galashev, K.A. Ivanichkina, K.P. Katin, M.M. Maslov, Computational study of lithium intercalation in silicene channels on a carbon substrate after nuclear transmutation doping, *Computation* 7 (2019) 60–76, <https://doi.org/10.3390/computation7040060>.
- A.Y. Galashev, O.R. Rakhmanova, Promising two-dimensional nanocomposite for the anode of the lithium-ion batteries. Computer simulation, *Physica E: Low-dim. Syst. Nanostruct.* 126 (2021) 114446–114456, <https://doi.org/10.1016/j.physe.2020.114446>.
- D.J. Evans, B.L. Holian, The Nose-Hoover thermostat, *J. Chem. Phys.* 83 (8) (1985) 4069–4074, <https://doi.org/10.1063/1.449071>.
- Y.-S. Choi, J.-H. Park, J.P. Ahn, J.-C. Lee, Interfacial reactions in the Li/Si diffusion couples: origin of anisotropic lithiation of crystalline Si in Li-Si batteries, *Sci. Rep.* 7 (2017) 14028, <https://doi.org/10.1038/s41598-017-14374-0>.
- Y. Pan, A. Gover, Spontaneous and stimulated radiative emission of modulated free-electron quantum wavepackets-semiclassical analysis, *J. Phys. Commun.* 2 (11) (2018) 115026, <https://doi.org/10.1088/2399-6528/aae2ec>.
- A.E. Galashev, A.A. Galasheva, Molecular dynamics simulation of copper removal from graphene by Bombardment with argon clusters, *High Energy Chem.* 48 (2) (2014) 112–116, <https://doi.org/10.1134/S0018143914020039>.
- J.L. Finney, A procedure for the construction of Voronoi polyhedra, *J. Comput. Phys.* 32 (1) (1979) 137–143, [https://doi.org/10.1016/0021-9991\(79\)90146-3](https://doi.org/10.1016/0021-9991(79)90146-3).
- A.E. Galashev, Structure of water clusters with captured methane molecules, *Rus. J. Phys. Chem. B* 8 (6) (2014) 793–800, <https://doi.org/10.1134/S1990793114110049>.
- A.K. Subramaniyan, C.T. Sun, Continuum interpretation of virial stress in molecular simulations, *Int. J. Solids Struct.* 45 (14-15) (2008) 4340–4346, <https://doi.org/10.1016/j.jisols.2008.03.016>.
- T. Siby, K.M. Ajith, Molecular dynamics simulation of the thermo-mechanical properties of monolayer graphene sheet, *Procedia Mater. Sci.* 5 (2014) 489–498, <https://doi.org/10.1016/j.mspro.2014.07.292>.
- Y. Yamada-Takamura, R. Friedlein, Progress in the materials science of silicene, *Sci. Technol. Adv. Mater.* 15 (6) (2014) 064404, <https://doi.org/10.1088/1468-6996/15/6/064404>.
- D. Drummond, V. Zolyomi, V.I. Fal'ko, Electrically tunable band gap in silicene, *Phys. Rev. B: Condens. Matter. Mater. Phys.* 85 (2012), 075423, <https://doi.org/10.1103/PhysRevB.85.075423>.
- A.E. Galashev, V.P. Skripov, Investigation on the disordering of argon hexagonal closed packed (HCP) crystals by the method of statistical geometry, *J. Struct. Chem.* 25 (5) (1985) 734–740, <https://doi.org/10.1007/BF00747917>.
- A.E. Galashev, V.P. Skripov, Stability of Lennard-Jones crystal structures in the molecular dynamics model, *J. Struct. Chem.* 26 (5) (1986) 716–721, <https://doi.org/10.1007/BF00773266>.

- [40] A.E. Galashev, V.P. Skripov, Stability and structure of a two-component crystal using a molecular dynamics model, *J. Struct. Chem.* 27 (3) (1986) 407–412, <https://doi.org/10.1007/BF00751820>.
- [41] A.E. Galashev, Incorrectness of the self-consistent field approximation for the argon crystal, *J. Struct. Chem.* 29 (2) (1988) 319–321, <https://doi.org/10.1007/BF00747997>.
- [42] Z. Zeng, X. Ma, J. Chen, Y. Zeng, D. Yang, Y. Liu, Effects of heavy phosphorus-doping on mechanical properties of Czochralski silicon, *J. Appl. Phys.* 107 (12) (2010) 123503, <https://doi.org/10.1063/1.3436599>.
- [43] A.Y. Galashev, Computational investigation of silicene/nickel anode for lithium-ion battery, *Solid State Ionics* 357 (2020) 115463–115474, <https://doi.org/10.1016/j.ssi.2020.115463>.
- [44] A.Y. Galashev, K.A. Ivanichkina, Computer study of atomic mechanisms of intercalation/ deintercalation of Li ions in a silicene anode on an Ag(111) substrate, *J. Electrochem. Soc.* 165 (9) (2018) A1788–A1796, <https://doi.org/10.1149/2.0751809jes>.
- [45] A.Y. Galashev, K.A. Ivanichkina, Computer test of a new silicene anode for lithium-ion batteries, *ChemElectroChem.* 6 (5) (2019) 1525–1535, <https://doi.org/10.1002/celec.v6.510.1002/celec.201900119>.
- [46] A.Y. Galashev, K.A. Ivanichkina, Computational investigation of a promising Si-Cu anode material, *Phys. Chem. Chem. Phys.* 21 (23) (2019) 12310–12320, <https://doi.org/10.1039/C9CP01571J>.
- [47] A.E. Galashev, Vitrification and structural differences between metal glass, quasicrystal, and Frank-Kasper phases, *J. Struct. Chem.* 37 (1) (1996) 120–136, <https://doi.org/10.1007/BF02578579>.
- [48] O.A. Novruzova, O.P. Rakhmanova, A.E. Galashev, The stability and structure of $(N_2)_j(H_2O)_i$ and $(Ar)_j(H_2O)_i$ clusters, *Rus. J. Phys. Chem. A* 81 (11) (2007) 1825–1828, <https://doi.org/10.1134/S0036024407110180>.
- [49] A.E. Galashev, Computer investigation of the structure of a porous SiO_2 nanoparticle under uniform tension, *Glass Phys. Chem.* 36 (5) (2010) 589–597, <https://doi.org/10.1134/S1087659610050081>.
- [50] Q.-X. Pei, Z.-D. Sha, Y.-Y. Zhang, Y.-W. Zhang, Effects of temperature and strain rate on the mechanical properties of silicene, *J. Appl. Phys.* 115 (2) (2014) 023519, <https://doi.org/10.1063/1.4861736>.